Three-dimensional reconstructions from cryoelectron microscopy images reveal an intimate complex between helicase DnaB and its loading partner DnaC

Carmen San Martin[1], Michael Radermacher[2], Bettina Wolpensinger[3], Andreas Engel[3], Caroline S Miles[4], Nicholas E Dixon[4] and José-María Carazo[1]*

Background: DNA helicases play a fundamental role in all aspects of nucleic acid metabolism and defects in these enzymes have been implicated in a number of inherited human disorders. DnaB is the major replicative DNA helicase in *Escherichia coli* and has been used as a model system for studying the structure and function of hexameric helicases. The native protein is a hexamer of identical subunits, which in solution forms a complex with six molecules of the loading protein DnaC. DnaB is delivered from this complex onto the DNA template, with the subsequent release of DnaC. We report here the structures of the DnaB helicase hexamer and its complex with DnaC under a defined set of experimental conditions, as determined by three-dimensional cryoelectron microscopy. It was hoped that the structures would provide insight into the mechanisms of helicase activity.

Results: The DnaB structure reveals that six DnaB monomers assemble as three asymmetric dimers to form a polar, ring-like hexamer. The hexamer has two faces, one displaying threefold and the other sixfold symmetry. The six DnaC protomers bind tightly to the sixfold face of the DnaB hexamer. This is the first report of a three-dimensional structure of a helicase obtained using cryoelectron microscopy, and the first report of the structure of a helicase in complex with a loading protein.

Conclusions: The structures of the DnaB helicase and its complex with DnaC reveal some interesting structural features relevant to helicase function and to the assembly of the two-protein complex. The results presented here provide a basis for a more complete understanding of the structure and function of these important proteins.

Addresses: [1]Centro Nacional de Biotecnología, Universidad Autónoma de Madrid, Cantoblanco, 28049 Madrid, Spain, [2]Max Planck Institute for Biophysics, Heinrich Hoffman Str. 7, 60528 Frankfurt, Germany, [3]Maurice E Mueller Institute, Biozentrum, Klingelbergstr 70, CH-4056 Basel, University of Basel, Switzerland and [4]Centre for Molecular Structure and Function, Research School of Chemistry, Australian National University, Canberra 0200, Australia.

*Corresponding author.
E-mail: carazo@cnb.uam.es

Key words: DNA helicase, DNA replication, *Escherichia coli*, protein structure, three-dimensional cryoelectron microscopy

Received: **16 December 1997**
Revisions requested: **21 January 1998**
Revisions received: **5 February 1998**
Accepted: **16 February 1998**

Structure 15 April 1998, **6**:501–509
http://biomednet.com/elecref/0969212600600501

Introduction

DNA helicases are ubiquitous enzymes with fundamental roles in all aspects of nucleic acid metabolism [1]. Their activity leads to disruption of hydrogen bonds between the two strands of duplex DNA, triggered by the energy of nucleoside 5′-triphosphate (NTP) hydrolysis. The unwinding reaction exhibits a specific polarity, which is expressed with respect to the strand of DNA on which the helicase is bound. Interest in the study of helicases is rising, as defects in more and more helicase genes are proved to be related to inherited human diseases [2].

Structural information on helicases has been difficult to obtain, and is still scarce. It is only in the last few years that the first high-resolution structures of helicases (all of them crystallized as monomers) have appeared [3–5]. Most DNA helicases, however, carry out their functions as multimeric complexes [1] and recent observations point to the existence of a subclass of these enzymes with a common hexameric structure [6,7]. In most cases these hexamers act as components of large protein assemblies. At present, no X-ray diffraction data for any hexameric helicase are available, although preliminary crystallization results have been reported for the plasmid RSF1010 RepA protein [8] and the helicase domain of bacteriophage T7 gene 4 protein (gp4) [9].

Escherichia coli has at least 12 different enzymes that act as helicases. Among them, DnaB is the main replicative helicase, the factor primarily responsible for the unwinding of the DNA duplex at replication forks in chromosomal DNA synthesis [10]. DnaB is a hexamer of identical subunits with a monomeric molecular weight of 52,259 Da. The protein unwinds double-stranded DNA by migrating in the 5′→3′ direction with respect to the strand to which it is bound. The DnaB helicase is a well established model system for the study of structure and function in the group of hexameric helicases, and recent work has yielded interesting data about its structural features at low resolution, based on electron microscopy studies of negatively stained specimens [11,12].

In solution, the hexameric DnaB forms a complex with six molecules of DnaC (27,935 Da/monomer). DnaC is

essential for replication *in vitro* and *in vivo*. The role of this protein centers around formation of the DnaB–DnaC complex, from which it delivers the helicase to its site of action on the DNA template. Upon delivery of DnaB, the DnaC protein is released from the protein–DNA complex [13,14]. Until now, no structural information has been available as regards to the way in which DnaB helicase and its loading companion DnaC interact with each other and with the DNA.

We have studied the structure of both the DnaB hexamer and the DnaB–DnaC complex by three-dimensional reconstruction of macromolecular aggregates from cryoelectron microscopy (cryoEM) images of frozen-hydrated specimens. This is the first report of the three-dimensional structure of a helicase obtained by this technique, and we also provide the first insight into the structure of a complex of a helicase with its loading protein.

Results

Electron microscopy and two-dimensional analysis of the DnaB hexamer and DnaB–DnaC complex

To avoid a possible source of heterogeneity in the images, both DnaB and DnaB–DnaC samples were prepared in a buffer containing ADP and Mg^{2+} at pH 7.6. Under these conditions, the tendency of the proteins to coexist in two (or more) conformational states is greatly reduced. The decreased stability of the DnaB–DnaC complex under these conditions was overcome during image processing by strict image classification of the data into homogeneous image data sets.

Input data for the three-dimensional reconstructions were collected following the random conical tilt scheme [15], with the tilted micrograph taken at 45° (Figures 1a and 1b). (It should be noted that the final angular assignment procedure described in the Materials and methods section indicated that the actual tilt range was substantially higher; Figure 2.) Sets of 3812 particle pairs were initially used for DnaB, and 1369 particle pairs were used for the DnaB–DnaC complex. Two-dimensional analysis of the selected populations showed that each of the two enzymatic complexes presented essentially a single view (end-on view) on the carbon support. Moreover, this view was very similar in dimensions and shape for the helicase and its complex with DnaC, both in cryoEM and negatively stained preparations (data not shown).

To rule out the possibility that dissociation of the DnaB–DnaC complex into DnaB hexamers and DnaC monomers had occurred, scanning transmission electron microscopy (STEM) mass measurements were determined with the same samples used for the three-dimensional reconstructions. Low dose dark field images of freeze-dried samples recorded at an acceleration voltage of 80 kV gave values after mass loss correction [16] of 334 ± 86 kDa (n = 520, where n = the number of particles used in the measurements) for DnaB and 509 ± 79 kDa (n = 650) for the DnaB–DnaC complex. These figures are in agreement with the molecular weights of both specimens and confirmed the integrity of the two protein complexes.

It was found that in both cases the end-on view of the particle had a characteristic and highly reproducible rotational power spectrum, with two clear peaks in the three- and sixfold harmonics (Figures 1c and 1d). In consequence, this feature was used to select the two homogeneous initial input sets from which low-resolution reference volumes were created for DnaB and the DnaB–DnaC complex. These volumes were used in further refinement steps as described in the Materials and methods section.

Three-dimensional reconstruction of the DnaB hexamer

A total number of 1498 particles were finally included in the three-dimensional reconstruction of the DnaB hexamer (Figure 3). This reconstruction has a resolution of 3.45 nm, as assessed by the differential phase residual method. Four main features of the reconstructed DnaB volume can be summarised. Firstly, the DnaB oligomer presents six density maxima arranged in a triangle-shaped particle. The edge of the triangle is 10–11 nm long; the external diameter of the particle is 12.5 nm, and the reconstructed height is 5.7 nm. Secondly, the six density lobes are organized in a ring around a channel running from face to face of the hexamer. The channel has a diameter of ~3 nm. Thirdly, the six subunits in the structure do not have the same aspect, as three of them seem significantly larger than the others (Figure 3d). Subunits with each of the two aspects are positioned alternately around the ring. Finally, direct observation of the volume (Figures 3a and 3c) and rotational analysis of the slices of the reconstruction (Figure 3b) reveal that the two faces of the hexamer are different, with a clear transition from sixfold to threefold symmetry between them.

Three-dimensional reconstruction of the DnaB–DnaC complex

The three-dimensional reconstruction of the DnaB–DnaC complex (Figure 4) was obtained in the same way as described for the DnaB hexamer. A total of 548 particles were included in the calculation of the final volume, which has a resolution of 4.22 nm. As for DnaB, the particle has a roughly triangle-shaped aspect. The DnaB–DnaC complex also displays a central channel running from face to face and, at this level of resolution, it has internal and external diameters almost indistinguishable from those of DnaB. The height of the reconstructed complex is 9.1 nm, however.

The reconstructed DnaB–DnaC particle presents several other interesting characteristics. Firstly, there is a clear twist of ~30° between the planes of the volume, as shown in

Figure 1

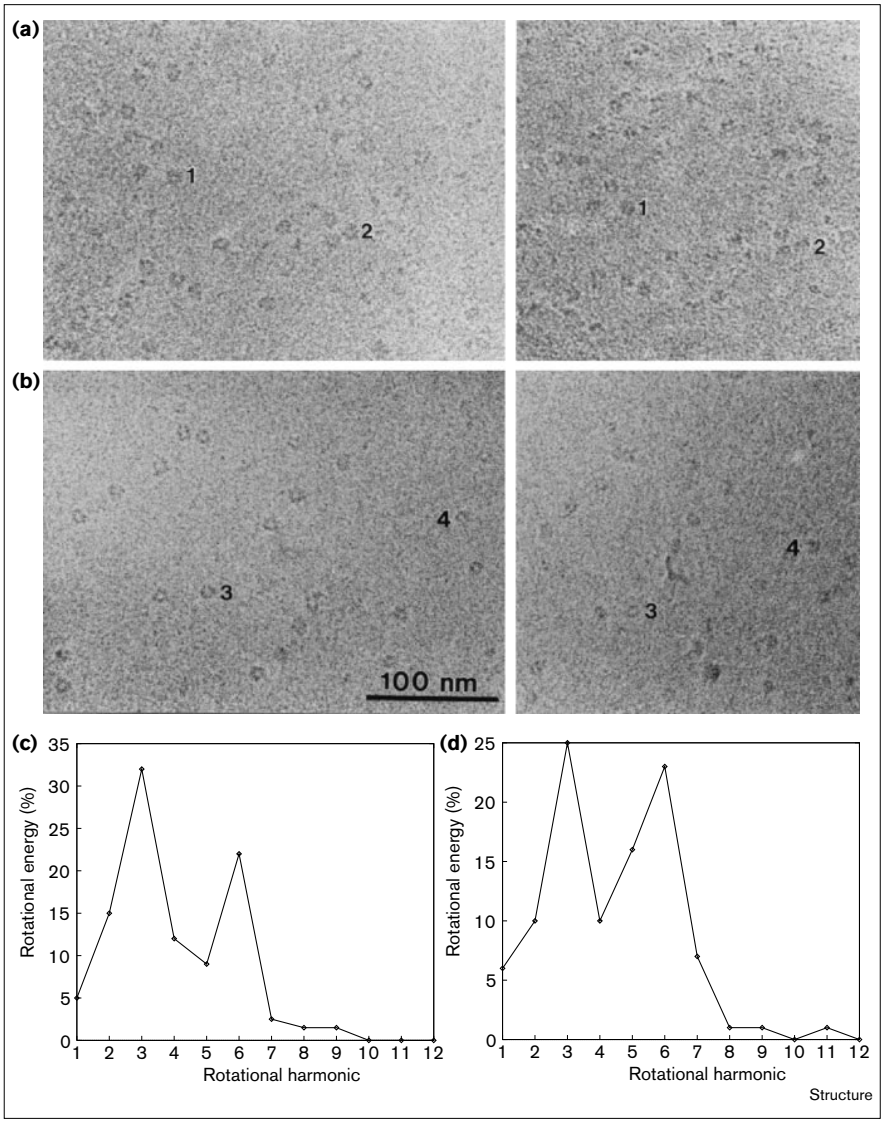

Cryoelectron microscopy images. Tilt pairs of frozen hydrated **(a)** DnaB and **(b)** the DnaB–DnaC complex. The three-dimensional reconstructions were calculated by means of the random conical tilting geometry for data collection with the tilted micrographs taken at 45°. The untilted micrographs are on the left, and the 45° tilted micrographs are on the right. Some particles and their counterparts in the tilted micrographs have been labelled with numbers. The scale bar represents 100 nm. **(c,d)** Rotational analysis of the average images of DnaB and the DnaB–DnaC complex, respectively, corresponding to the total population of initially selected particles. The rotational spectra were calculated between radii 4.2 and 6.8 nm.

Figure 4c. The twist can also be directly observed, for example, by comparison of slices 11 and 17 in Figure 4a. Secondly, the rotational analysis of the DnaB–DnaC volume slices shows differences in the relative weight of the sixfold and threefold components along the axis of the channel, although in general the threefold symmetry is more prominent than in the study of DnaB alone (Figure 4b). It is noticeable, however, that this rotational energy plot presents an area very similar to that of the DnaB hexamer (compare the right-hand side of the plots in Figures 3b and 4b). The similarity ends just at the region of the volume where the sixfold symmetry should start to prevail (approximately around slice 20 in DnaB–DnaC and slice 10 in DnaB). On the other hand, the opposite end of the plot in Figure 4b shows a general behaviour similar to that of DnaB (threefold to sixfold transition), but along a shorter height (slices 5 to 11). These symmetry data offer information on how the six DnaC monomers are bound to the DnaB helicase ring, as discussed in the next section.

Discussion

DnaB helicase

When observed at pH 7.6 in the frozen hydrated state, the DnaB helicase and its complex with DnaC presented a very similar end-on view: a ring-like particle with threefold and sixfold symmetries. These views of the two specimens were virtually indistinguishable in size and shape, even after two-dimensional image processing. This raised the possibility that the DnaB–DnaC complex had dissociated, so a STEM mass measurement study was used to confirm the integrity of the particles. The three-dimensional reconstructions were then calculated using a random conical tilting data

Figure 2

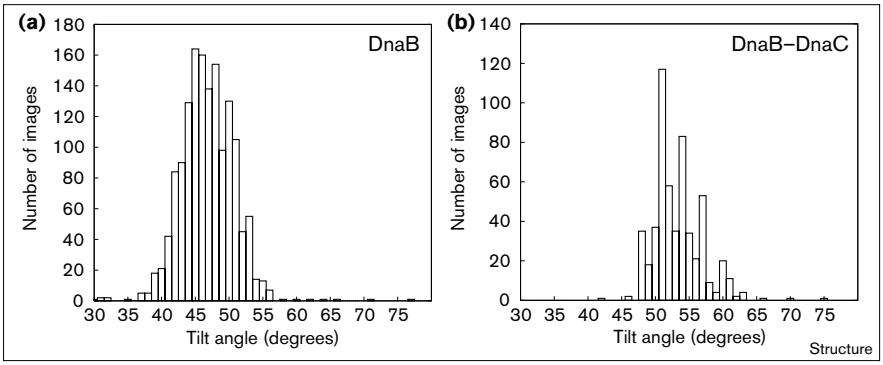

Histograms of the final tilt angles obtained after the refinement process for both the three-dimensional reconstruction of **(a)** DnaB and **(b)** the DnaB–DnaC complex.

collection geometry and an ART-based reconstruction algorithm, along with a three-dimensional Radon transform based method to find the orientation of the projections.

The three-dimensional reconstruction of the DnaB hexamer in ice essentially confirms the structural features already found in the three-dimensional reconstruction of the particle from negatively stained preparations [11]. In agreement with its hexameric character, the DnaB oligomer presents six density maxima, but organized in a triangle-shaped particle. As previously proposed [11], this arrangement strongly suggests assembly of the hexamer as a trimer of dimers. Moreover, in the reconstruction obtained from cryoEM data the putative dimers seem to be asymmetric, with one of every two lobes in the particle being significantly larger than the other. This implies that, in spite of being biochemically identical, the DnaB monomers adopt different orientations, or even different conformations, when assembled into the hexamer. This result might explain aspects of the cooperative binding of ATP by the DnaB hexamer, which occurs in a biphasic manner [17], and suggests that the oligomeric organization of the functional complex of the helicase has C3 symmetry.

A C3 model for the assembly of the DnaB monomers in the hexamer had been proposed in [11], based both on the negative staining reconstruction of the particle and on a previously proposed monomer model [18]. Later, Yu and collaborators [12] expanded this model in order to explain a C3/C6 polymorphism found in their DnaB samples. This kind of polymorphism has not been found in the samples used for the three-dimensional reconstructions reported here, but current work in our group has detected it both in other related helicases (M Bárcena, CSM, F Weise, S Ayora, JC Alonso and JMC, unpublished data) and in DnaB samples prepared under different conditions: the quaternary state of the DnaB hexamer is pH-dependent. At pH 7.6 (as in the cryoEM buffer), the C3 form is the only one detected by negative staining while at lower pH values both C3 and C6 forms coexist. The proportion of DnaB particles exhibiting C6 symmetry increases as the pH decreases reaching a point where C3 particles are no longer detected (LE Donate, personal communication). The results presented here clearly suggest that an architecture based on the existence of asymmetric dimers should be considered when modelling the structure of this macromolecule.

The structural model that better encompasses all of these observations would therefore be a mixed C3/C6 model. This kind of hybrid symmetry has already been proposed for the transcription termination factor Rho from *E. coli* [19], on the grounds of cross-linking experiments. It is expected that further studies on the functional significance of, and the transitions between, the C3 and C6 states will shed light on the mechanism of action of hexameric helicases.

The reconstruction of the DnaB hexamer in ice also confirms the existence of a channel about the threefold axis. The channel is fully open at both ends of the particle, and has a diameter of ~3 nm. It has already been proposed, on the basis of both structural [11] and biochemical [20] studies, that this channel is involved in the interaction of the DnaB enzyme with its DNA substrate. This kind of interaction seems to be a common feature in hexameric helicases: it has also been suggested for the SV40 large T antigen [21,22], the phage T4 helicase gp41 [23], and the RuvB helicase from *E. coli* [24], and proved for the case of the phage T7 helicase–primase complex [25]. Furthermore, recent work on the T7 gene 4 helicase [26,27] prooves that in this case the 5′ to 3′ strand of the DNA traverses the center of the helicase ring, while the other strand is excluded. In addition, it has been shown that one hexamer of DnaB binds a 20-mer of single-stranded DNA [20]. The channel in our reconstruction of the DnaB oligomer has a length of 5.7 nm, which is sufficient to accommodate this length of DNA.

The height of the reconstructed volume (5.7 nm) is noticeably different from the reconstructed height measured by

Figure 3

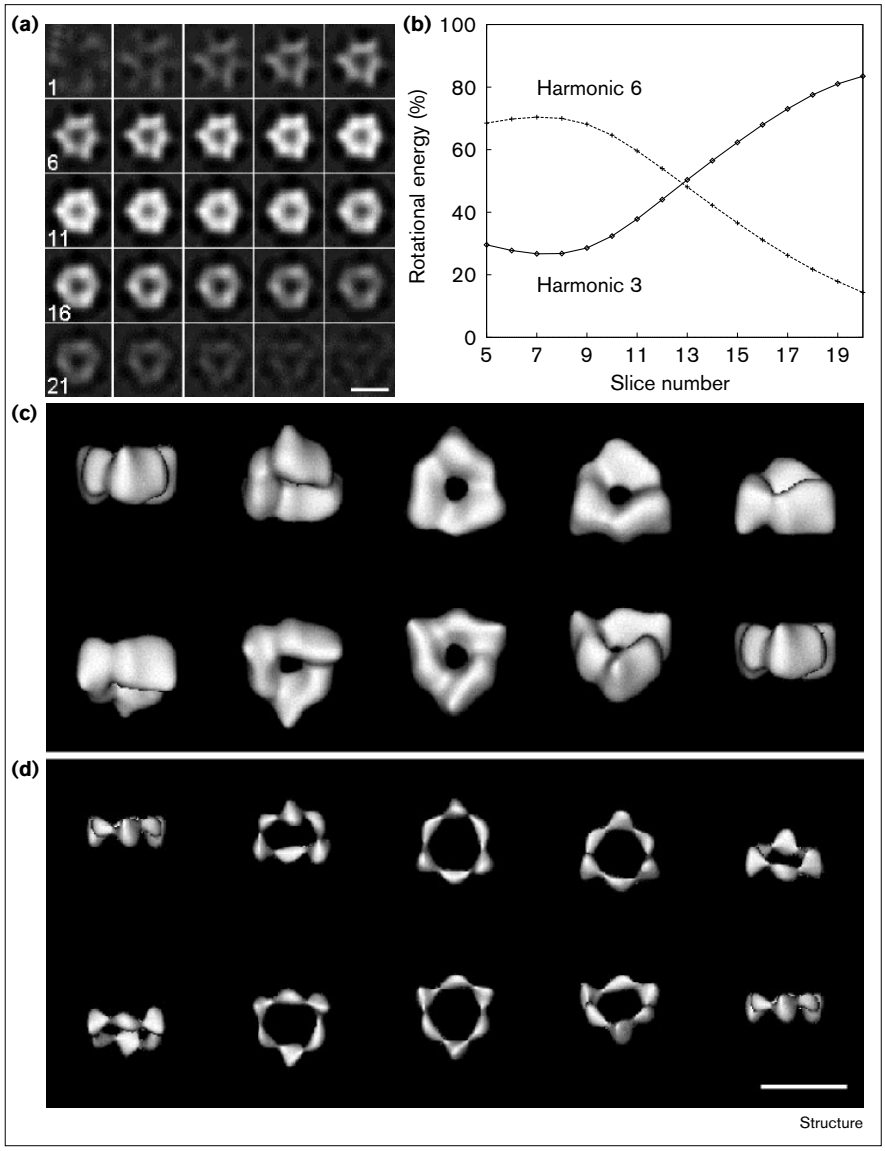

Three-dimensional reconstruction of the DnaB hexamer. **(a)** Slices through the reconstruction. **(b)** Variation in the rotational energy corresponding to harmonics 3 and 6 among successive slices of the reconstruction. **(c)** Surface rendering of the volume at a threshold value including 100% of the protein mass. The particle is represented (from top left to bottom right) as rotating around an axis parallel to the specimen support; in this representation the axis would be a horizontal line on the page. **(d)** Surface rendering of the volume at a higher threshold (14% of the expected mass), emphasizing the highest density areas and the contacts between them. The scale bars represent 10 nm.

analysis of negative staining data (3.8 nm) [11]. This clearly reflects the flattening suffered by the specimen under dehydration conditions. Using analytical ultracentrifugation experiments, Bujalowski and collaborators [28] modelled the DnaB oligomer as an ellipsoid with an axial ratio of 2.6 ± 0.6. In the three-dimensional reconstruction reported here, with a particle of 12.5 nm diameter and 5.7 nm height, this ratio would be 2.2.

The last relevant characteristic deducible from the three-dimensional reconstruction of DnaB, which was already pointed out in [11], is the structural polarity of the particle. It is clear from direct observation of the volume that the two faces of the hexamer are different, but this difference becomes even more evident after calculation of the rotational spectra of the volume slices. These calculations show a distinct transition between sixfold and threefold symmetries as one traverses through the particle. This is a particularly interesting feature, given the unidirectionality of the helicase translocation during the unwinding reaction, and has already been noted in negative staining studies of other hexameric helicases, including the T7 helicase–primase complex [29] and the SV40 large T antigen [21]. This structural polarity suggests a mechanism for the interaction of the helicase with single-stranded DNA in a preferred direction. Such a mechanism would facilitate binding to the substrate in a defined orientation, and its advance in a preferred direction into the replication fork, possibly by means of ATP hydrolysis-driven conformational changes.

Figure 4

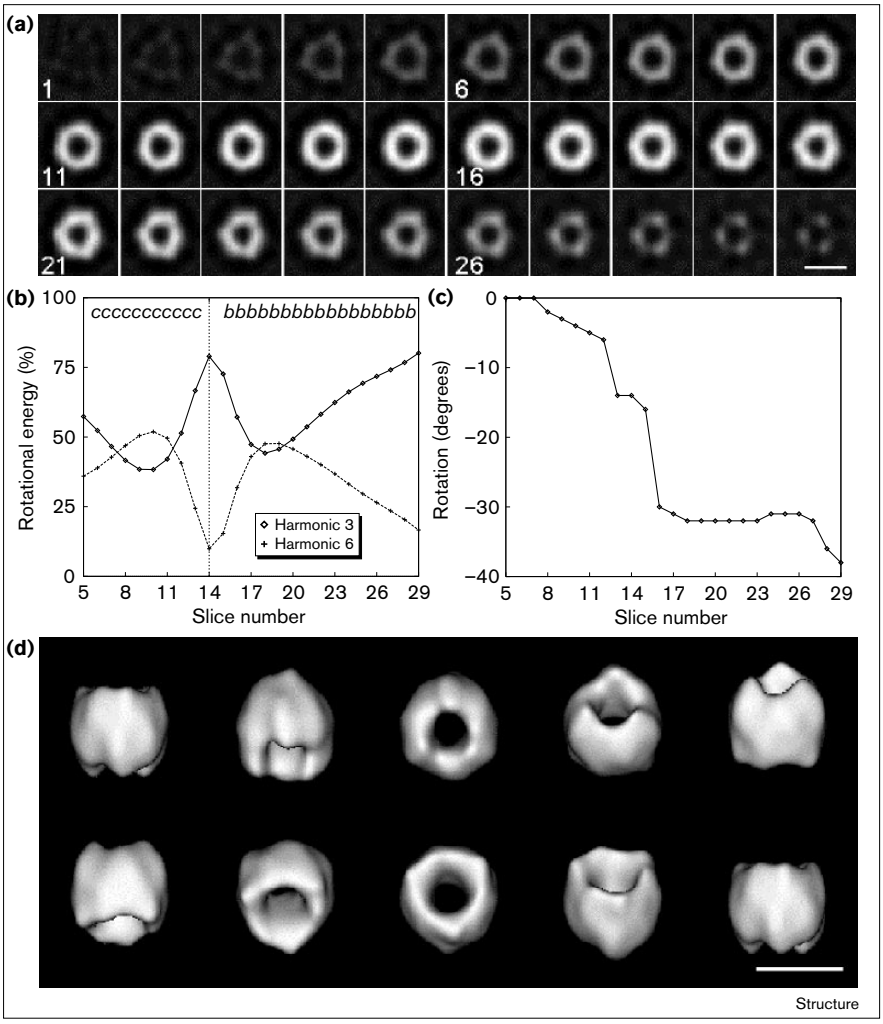

Three-dimensional reconstruction of the DnaB–DnaC complex. **(a)** Slices through the reconstruction. **(b)** Variation in the rotational energy corresponding to harmonics 3 and 6 among successive slices of the reconstruction. The letters *b* and *c* indicate tentative assignment of the particle volumes occupied by DnaB and DnaC, respectively. **(c)** The structural twist of successive slices in the reconstruction, measured as a rotation relative to the the first slice judged to contain significant information (slice number 5). **(d)** Surface rendering of the volume at a threshold value including 100% of the protein mass. The scale bars represent 10 nm.

There is, however, a quite remarkable difference between the negative staining reconstruction of the DnaB hexamer shown in [11] and the results presented here. In the negatively stained sample, the triangular aspect of the particle was mainly due to the existence of three small density areas located on its periphery. These small lobes do not appear in the reconstruction from frozen hydrated samples, where the threefold symmetry arises from one of every two lobes in the hexamer being significantly larger than the other. There are two possible causes for this discrepancy. On one hand, the size of the small lobes makes them fall in a frequency range where the contrast transfer function (CTF) of the microscope is almost zero under the defocus conditions used to acquire the cryoEM micrographs. This, in addition to the low resolution of the cryoEM reconstruction, could have led to loss of these details from the volume. On the other hand, however, the small lobes could have been produced in the negative staining images as a consequence of deformations suffered by the most flexible areas of the particle during the collapse induced by staining and dehydration. A simulation of the effect of the CTF and low pass filtration (to 3.45 nm) of the negative staining reconstruction from [11] produced a blurring and weakening of the three external lobes, but did not give conclusive results. Thus, with the data available at present it is not possible to distinguish between these two possibilities; more work is required to clarify this problem.

The DnaB–DnaC complex

The three-dimensional reconstruction of the DnaB–DnaC complex showed a particle very similar to that of the DnaB hexamer alone, at least at the resolution reached with cryoEM. The main difference between the reconstructed helicase and its complex with DnaC lies in the height of the particles: 5.7 nm for DnaB and 9.1 nm for the DnaB–DnaC complex. The height ratio between the two specimens is thus 1.6, which is practically the same value as their mass ratio of 1.5. Observation of the slices of the

Figure 5

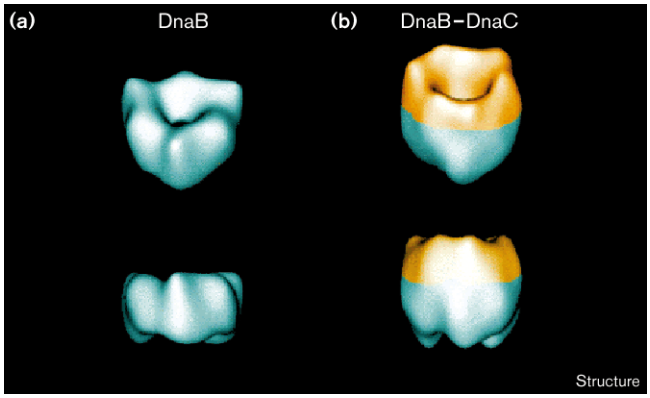

Comparison of the reconstructed volumes of DnaB and the DnaB–DnaC complex. **(a)** Two views of DnaB shown in blue. **(b)** Two corresponding views of the DnaB–DnaC complex presented in blue and gold (the blue colour is used to mark the region assigned to the DnaB protein alone, while the gold is used for the area assigned to DnaC).

volume shows that the DnaB–DnaC complex is organized as a ring throughout the whole particle. In consequence, it appears that the six DnaC monomers are accommodated themselves as a ring on top of one of the two faces of the DnaB hexamer. This explains the similarity between the end-on views of the two particles.

There is another relevant feature in the reconstructed DnaB–DnaC complex, namely, the structural twist among the slices of the volume. This result implies that each one of the six monomers of DnaC are interacting with two monomers of DnaB (and *vice versa*) in a ring-like configuration. Furthermore, if we assume — based on the similarity of their end-on views and the rotational analysis of the slices of the two specimens described — that both the DnaB hexamer and the DnaB–DnaC complex have the same orientation on the carbon support, then DnaC would be interacting with DnaB over the region where the sixfold symmetry of DnaB is more prevalent. The six DnaC monomers would also be adopting a polar ring conformation in the complex, meaning that the face in contact with DnaB would be a sixfold ring while the 'external' face presents threefold symmetry. It would be expected that the central area of the volume (slices 11 to 17] would not show the sixfold symmetry because of the blurring induced by the interlocking of the DnaB and DnaC monomers. It is in this same area that the structural twist described above takes place. Based on these considerations, a tentative assignment of the particle areas occupied by DnaB and DnaC has been indicated in Figure 4b and Figure 5. In summary, this reconstruction of the DnaB–DnaC complex points to a very close interaction between the helicase and its loading partner, with protein–protein interactions occurring over an extensive contact surface.

Biological implications

The mechanism of action of hexameric helicases is still an unsolved problem, in spite of the critical role of these enzymes in all processes of DNA metabolism and the amount of biochemical knowledge in the field. Defects in the genes for these proteins have been shown to be related to a number of human inherited diseases and their further study is therefore of much current interest. Structural knowledge should provide a better understanding of these important enzymes.

We report here a cryoelectron microscopy study of the three-dimensional structures of the DnaB helicase and its complex with DnaC. The structures provide new and interesting data relating to the quaternary structure of the helicase functional complex and its association with the loading protein, DnaC. The DnaB structure confirms the presence of structural characteristics in the DnaB oligomer relevant to its activity: a channel running through the hexamer, probably involved in interaction with the DNA substrate, and a defined polarity, which could be related to the polarity of helicase action. The structure also shows that the six DnaB protomers associate as three asymmetric dimers in a triangle-shaped particle with C3 symmetry. Integration of this result with previously reported studies suggests the possibility of a mixed C3/C6 symmetry model for the DnaB hexamer.

DnaC is responsible for loading the helicase onto the DNA substrate in the correct orientation; the DnaB oligomer forms a complex with six DnaC molecules. The three-dimensional reconstruction of the DnaB–DnaC complex indicates that the six DnaC protomers are assembled as a ring onto the sixfold face of the DnaB hexamer, each DnaC molecule interacting with two DnaB monomers. This work provides the first report on the interactions between a helicase and its loading partner.

Materials and methods

Protein purification

E. coli strain AN1459/pPS560 [11] was used as source of DnaB and DnaC proteins. DnaB was purified as described [11], except that it was separated from DnaC and small amounts of the DnaB–DnaC complex by chromatography on a column of DEAE Fractogel (Merck) in the presence of Mg^{2+} and ADP instead of ATP. The protein was then further purified by elution from a column of Macro-Prep Ceramic Hydroxyapatite (BioRad) with phosphate buffer (pH 7.2), containing Mg^{2+} and ADP [30]. The DnaB–DnaC complex was reassembled during dialysis of a mixture of partially purified samples of DnaB and DnaC (from DEAE Fractogel chromatography) in Tris buffer containing 5 mM $MgCl_2$ and 0.1 mM ATP. The DnaB–DnaC complex was then separated completely from DnaB and DnaC and freed of other contaminants by chromatography on a DEAE Fractogel column in the presence of Mg^{2+} and ATP [30].

CryoEM

For the cryoEM studies, the protein samples were diluted (>50-fold) to 40 μg/ml in 50 mM Tris.HCl pH 7.6, 2 mM DTT, 5 mM $MgCl_2$, 200 mM NaCl, 0.25 mM ADP. Samples were adsorbed onto carbon-coated molybdenum holey grids after 30 s of glow discharge, and vitrified by

quick plunging in liquid ethane in a double-side blotting device [31]. CryoEM was carried out in a Philips EM 420 equipped with a low dose device, Gatan cryostage and cryotransfer system, at 100 kV accelerating voltage and 60,000× magnification. Tilt pairs were taken in Kodak SO-163 plates with 10 e/Å^2 dose, using defocus values of 1.5 μm (in the center of the plate) for the 45° tilted image and 2 μm for the untilted image.

STEM

For mass analysis by STEM [32], DnaB or the DnaB–DnaC complex were adsorbed to glow discharged grids covered with a carbon film (3 nm in thickness) mounted on a fenestrated plastic film, and washed with four drops of double-distilled water. Grids were plunged into liquid nitrogen and freeze-dried within the pretreatment chamber attached to a Vacuum Generator HB5 STEM at −80°C. Elastic annular dark-field images containing 512 × 512 pixels were acquired in digital format at 80 kV, at 200,000 × (pixel size 0.93 nm) magnification and at an average dose of 300 electrons/nm^2. Digital acquisition of the microscope parameters and image data, system calibration and mass analysis were carried out as previously described [16].

Two-dimensional image processing

Micrographs were digitized in an Eikonix IEEE 488 camera with a pixel size of 0.38 nm in the sample. Particle selection and two-dimensional analysis (classification and alignment) were performed as described [21] using the Xmipp software package [33]. Only one prevalent view could be detected in the micrographs. A total of 3812 DnaB particles and 1369 DnaB–DnaC particles corresponding to this preferred view were selected in this way.

Several state-of-the-art classification techniques (self-organizing maps, multivariate statistical analysis, hierarchical methods) [34] were applied to the untilted particles after alignment, in an attempt to find different views or homogeneous subsets of the specimens to proceed with the three-dimensional reconstructions. Finally, after realizing that the symmetry pattern was a highly reproducible characteristic of the two populations, a homogeneous subset of images (548 particle images of DnaB and 217 of DnaB–DnaC) was extracted from each sample (DnaB and DnaB–DnaC) by multivariate statistical analysis of the rotational spectra of single particles [35]. The rotational spectra were calculated between radii 1.6 and 6.8 nm. In this way, those particles with rotational energy spectra mainly concentrated in the threefold and sixfold harmonics were chosen as the starting data set for the three-dimensional reconstructions.

Three-dimensional reconstruction

The three-dimensional reconstructions were calculated by means of an algebraic reconstruction technique (ART) algorithm [36] using smooth spherical functions as bases elements. This algorithm has been shown quantitatively to reduce the appearance of artificial elongations along the direction perpendicular to the grid plane when compared to other algorithms commonly used in the field for the case of a conical tilt data collection geometry [36] (for other situations, specifically a single axis tilt data collection geometry, this elongation reduction has also been reported [37]).

A three-dimensional Radon transform (RT) based system [38], integrated in the SPIDER software package [39], was used in an iterative way both for centering and angular refinement of the tilted projections.

The starting point was the subset of tilted images (548 particle images of DnaB and 217 of DnaB–DnaC) which had been selected as homogeneous, based on classification methods applied to the zero degree images. The tilting and azimuth angles were assigned to these images as in the classical random conical tilting scheme (i.e. as found in the analysis of data from a random conical tilt experiment during particle selection and two-dimensional alignment of the zero degree images, respectively). No previous translational alignment was applied to the tilted images.

Refinement of the projection alignments was done using a dynamic reference alignment [40]. In dynamic reference alignment schemes the reference is updated after each alignment step. Radon transform based alignments were used here, because only these techniques allow for an easy and accurate updating of the three-dimensional reference. In contrast, to provide a three-dimensional reference volume with correct scaling reprojection methods would require a complete reconstruction algorithm to be carried out after alignment of each single projection.

Initially, a low-resolution reference volume was created as described. The two-dimensional RT of every image was calculated in two degree increments and Fourier transformed. These two-dimensional Fourier Radon transforms (FRTs) were placed in the three-dimensional space following the central section theorem. Lines that are common to multiple projections are averaged in this procedure. The resulting three-dimensional FRT was used as a first reference in the dynamic reference alignment. The alignment was applied to one projection at a time. The projection that is being aligned is first 'subtracted' from the three-dimensional reference FRT. For this subtraction each single line L(i) in the three-dimensional reference that lies in the section that corresponds to this projection is multiplied by the number N(i) of common lines that had been averaged to form this line. The FRT of the projection is then subtracted and the lines in the section are divided by (N(i)−1). The same section, with the current projection subtracted is used as the reference for translational alignment of the two-dimensional FRT by cross-correlation. The shift is applied to the two-dimensional FRT by phase multiplication. The shifted two-dimensional FRT is then averaged back into the section. This operation was repeated four times, starting with a new reference volume in each iteration created from all projections aligned in the previous step. This recalculation of the reference was done to minimize the accumulation of numerical errors.

The angular values were refined in the same way. Here also the FRT of each projection was subtracted from the three-dimensional FRT before alignment, and averaged back into the three-dimensional FRT after alignment. As this was an angular refinement, the section from which the projection was subtracted had a different direction to the section into which the projection was averaged after angular refinement.

As a reference volume we used the volume built with the centered projections, and then a search was carried out for correlation maxima in a ±15 degree interval, with three degree increments, for the three Euler angles which define the orientation of each projection in the space. Five refinement iterations were performed in this way. The centering refining cycle was repeated twice, finishing with a new translational alignment. In every case (for both centering and angular refinement), previous knowledge about the rotational symmetry of the specimen was used to build the reference volumes and to search for the correlation maxima. This meant that because of the threefold symmetry of the particles, each projection was added or subtracted from the volumes three times, in positions related by 120° rotations around the symmetry axis (i.e. in the azimuth angle).

Finally, many of the initially discarded projections (possibly slightly rocked views) were incorporated into the volume, and the angular refinement was repeated. The correlation coefficients of the new projections, when aligned and cross-correlated to the reference volume, were used to decide which projections would be included in the final reconstruction. In the end, approximately 50% of the particles selected initially (1369 for DnaB and 548 for the DnaB–DnaC complex) were used in the three-dimensional reconstructions. The final distribution of tilt angles corresponding to the refined geometry of the sets of DnaB and DnaB–DnaC particles is presented in Figure 2. By this procedure, the resolution was improved from 4.2 to 3.45 nm in the case of DnaB, and from 5.4 to 4.2 nm for the DnaB–DnaC complex. This process also introduced additional information in the missing cone region, as a reduction of vertical blurring was observed for the DnaB hexamer.

Resolution was calculated using the differential phase residual method, by comparing each volume with itself after a 120° rotation around the

threefold axis. A threefold symmetry was imposed on the final reconstructions after filtration to the estimated resolution. Surface rendering representations were displayed using the program WEB [39] at threshold values representing 100% of the expected volume for each specimen (assuming a mean protein density of 1.33 g/cm^3), and then at higher threshold values to allow better observation of the highest protein density areas.

Acknowledgements

The authors wish to thank J Frank for use of the cryoEM facilities at the Wadsworth Center (Albany, NY) and R Grassucci for expert help with the cryoEM. Earlier versions of this draft were commented on by JL Carrascosa, JM Valpuesta and SA Muelle, whose efforts are greatly appreciated. This work was supported in part by Grant BIO95-0768 from the Comisión Interministerial de Ciencia y Tecnología (CICYT), Spain (to JMC) and by NSF grant DBI 9515518 (to MR). The last collaborative works between JMC and MR were supported by a joint German/Spanish grant HA 1997-0049.

References

1. Lohman, T.M. & Bjornson, K.P. (1996). Mechanism of helicase-catalyzed DNA unwinding. *Annu. Rev. Biochem.* **65**, 169-214.
2. Ellis, N.A. (1997). DNA helicases in inherited human disorders. *Curr. Opin. Gen. Develop.* **7**, 354-363.
3. Subramanya, H.S., Bird, L., Brannigan, J.A. & Wigley, D. (1996). Crystal structure of a Dexx box DNA helicase. *Nature* **384**, 379-383.
4. Korolev, S., Hsieh, J., Gauss, G.H., Lohman, T.M. & Waksman, G. (1997). Major domain swivelling revealed by the crystal structures of binary and ternary complexes of *E.coli* Rep helicase bound to single-stranded DNA and ADP. *Cell* **90**, 635-647.
5. Yao, N., Hesson, T., Cable, M., Hong, Z., Kwong, A., Lee, H. & Weber, P.C. (1997). Structure of the hepatitis C virus RNA helicase domain. *Nat. Struct. Biol.* **4**, 463-467.
6. Marians, K.J. (1997). Helicase structures: a new twist on DNA unwinding. *Structure* **5**, 1129-1134.
7. West, S.C. (1996). DNA helicases: new breeds of translocating motors and molecular pumps. *Cell* **86**, 177-180.
8. Röleke, D., Hoier, H., Bartsch, C., Umbach, P., Scherzinger, E., Lurz, R. & Saenger, W. (1997). Crystallization and preliminary X-ray crystallographic and electron microscopic study of a bacterial DNA helicase (RSF1010) *RepA. Acta Cryst. D* **53**, 213-216.
9. Bird, L.E., Hakansson, K., Pan, H. & Wigley, D.B. (1997). Characterization and crystallization of the helicase domain of bacteriophage T7 gene 4 protein. *Nucleic Acids Res.* **25**, 2620-2626.
10. Matson, S.W. (1991). DNA helicases of *Escherichia coli. Prog. Nucleic Acids Res. Mol. Biol.* **40**, 289-326.
11. San Martin, M.C., Stamford, N.P.J., Dammerova, N., Dixon, N.E. & Carazo, J.M. (1995). A structural model for the *Escherichia coli* DnaB helicase based on electron microscopy data. *J. Struct. Biol.* **114**, 167-176.
12. Yu, X., Jezewska, M.J., Bujalowski, W. & Egelman, E.H. (1996). The hexameric *E. coli* DnaB helicase can exist in different quaternary states. *J. Mol. Biol.* **259**, 7-14.
13. Wahle, E., Lasken, R.S. & Kornberg, A. (1989). The DnaB–DnaC replication protein complex of *Escherichia coli.* I. Formation and properties. *J. Biol. Chem.* **264**, 2463-2468.
14. Allen, G.C., Jr. & Kornberg, A. (1991). Fine balance in the regulation of DnaB helicase by DnaC protein in replication in *Escherichia coli. J. Biol. Chem.* **266**, 22096-22101.
15. Radermacher, M., Wagenknecht, T., Verschoor, A. & Frank, J. (1987). Three-dimensional reconstruction from a single-exposure, random conical tilt series applied to the 50S ribosomal subunit of *Escherichia coli. J. Microsc.* **146**, 113-136.
16. Müller, S.A., Goldie, K.N., Buerki, R., Haering, R. & Engel, A. (1992). Factors influencing the precision of quantitative scanning transmission electron microscopy. *Ultramicroscopy* **46**, 317-334.
17. Bujalowski, W. & Klonowska, M.M. (1993). Negative cooperativity in the binding of nucleotides to *Escherichia coli* replicative helicase DnaB protein. Interactions with fluorescent nucleotide analogs. *Biochemistry* **32**, 5888-5900.
18. Nakayama, N., Arai, N., Kaziro, Y. & Arai, K. (1984). Structural and functional studies of the *dnaB* protein using limited proteolysis: characterization of domains for DNA-dependent ATP hydrolysis and for protein association in the primosome. *J. Biol. Chem.* **259**, 88-96.
19. Horiguchi, T., Miwa, Y. & Shigesada, K. (1997). The quaternary geometry of transcription termination factor rho: assignment by chemical cross-linking. *J. Mol. Biol.* **269**, 514-528.
20. Bujalowski, W. & Jezewska, M.J. (1995). Interactions of *Escherichia coli* primary replicative helicase DnaB protein with single-stranded DNA. The nucleic acid does not wrap around the protein hexamer. *Biochemistry* **34**, 8513-8519.
21. San Martin, M.C., Gruss, C. & Carazo, J.M. (1997). Six molecules of SV40 large T antigen assemble in a propeller-shaped particle around a channel. *J. Mol. Biol.* **268**, 15-20.
22. Dean, F.B., Borowiec, J.A., Toshihiko, E. & Hurwitz, J. (1992). The simian virus 40 T antigen double hexamer assembles around the DNA at the replication origin. *J. Biol. Chem.* **267**, 14129-14137.
23. Dong, F., Gogol, E.P. & von Hippel, P.H. (1995). The phage T4-coded DNA replication helicase (gp41) forms a hexamer upon activation by nucleoside triphosphate. *J. Biol. Chem.* **270**, 7462-7473.
24. Stasiak, A., Tsaneva, I.R., West, S.C., Benson, C.J.B., Yu, X. & Egelman, E.H. (1994). The *Escherichia coli* RuvB branch migration protein forms double hexameric rings around DNA. *Proc. Natl. Acad. Sci. USA* **91**, 7618-7622.
25. Yu, X., Hingorani, M.M., Patel, S.S. & Egelman, E.H. (1996). DNA is bound within the central hole to one or two of the six subunits of the T7 DNA helicase. *Nat. Struct. Biol.* **3**, 740-743.
26. Ahnert, P. & Patel, S.S. (1997). Asymmetric interactions of the hexameric bacteriophage T7 DNA helicase with the 5′and 3′-tails of the forked DNA substrate. *J. Biol. Chem.* **272**, 32267-32273.
27. Jezewska, M.J., Surendran, R. & Bujalowski, W. (1997). Strand specificity in the interactions of *Escherichia coli* primary replicative helicase DnaB protein with a replication fork. *Biochemistry* **36**, 10320-10326.
28. Bujalowski, W., Klonowska, M.M. & Jezewska, M.J. (1994). Oligomeric structure of *Escherichia coli* primary replicative helicase DnaB protein. *J. Biol. Chem.* **50**, 31350-31358.
29. Egelman, E.H., Yu, X., Wild, R., Hingorani, M.M. & Patel, S.S. (1995). Bacteriophage T7 helicase/primase proteins form rings around single-stranded DNA that suggest a general structure for hexameric helicases. *Proc. Natl. Acad. Sci. USA* **92**, 3869-3873.
30. Dammerova, N. (1995). Towards the structure of the *Escherichia coli* DnaB helicase. PhD thesis, Australian National University, Canberra, Australia.
31. Cyrklaff, M., Adrian, M. & Dubochet, J. (1990). Evaporation during preparation of unsupported thin vitrified aqueous layers for cryo-electron microscopy. *J. Electron Microsc. Tech.* **16**, 351-355.
32. Engel, A. & Colliex, C. (1993). Application of scanning transmission electron microscopy to the study of biological structure. *Curr. Opin. Biotech.* **4**, 403-411.
33. Marabini, R., *et al.,* & Carazo, J.M. (1996). Xmipp: an X-Windows based image processing package for electron microscopy. *J. Struct. Biol.* **116**, 237-240.
34. Frank, J. (1996). Multivariate statistical analysis and classification of images. In *Three-Dimensional Electron Microscopy of Macromolecular Assemblies*. pp. 126-181, Academic Press Limited, London, UK.
35. Crowther, R.A. & Amos, L.A. (1971). Harmonic analysis of electron microscope images with rotational symmetry. *J. Mol. Biol.* **60**, 123-130.
36. Marabini, R., Herman, G.T. & Carazo, J.M. (1998). 3D reconstruction in electron microscopy using ART with smooth spherically symmetric volume elements (blobs). *Ultramicroscopy*, in press.
37. Marabini, R., Rietzel, E., Rchroeder, R., Carazo, J.M. & Herman, G.T. (1998). Three-dimensional reconstruction from reduced sets of very noisy images acquired following a single axis-tilt schema: application of a new three-dimensional reconstruction algorithm and objective comparison with weighted backprojection. *J. Struct. Biol.,* in press.
38. Radermacher, M. (1994). Three-dimensional reconstruction from random projections: orientational alignment via Radon transforms. *Ultramicroscopy* **53**, 121-136.
39. Frank, J., Radermacher, M., Penczek, P., Zhu, J., Li, Y., Ladjadj, M. & Leith, A. (1996). SPIDER and WEB: processing and visualization of images in 3D electron microscopy and related fields. *J. Struct. Biol.* **116**, 190-199.
40. Radermacher, M. (1998). Radon transform techniques for alignment and 3D-reconstruction from random projections. *Scanning Micros. Int. Suppl.*, in press.